Applied Physics A (2019) 125:301
https://doi.org/10.1007/s00339-019-2608-7

Applied Physics A
Materials Science & Processing

Large electrostrictive properties in lead-free $BaTiO_3$–$ZnSnO_3$ solid solutions

Yinyin Zhu[1]

Received: 1 March 2019 / Accepted: 31 March 2019 / Published online: 6 April 2019

Abstract
A new lead-free perovskite piezoelectric solid solution $(1-x)BaTiO_3$–$xZnSnO_3$ (BT–xZS) was designed and fabricated using the traditional solid-state reaction method. The introduction of $ZnSnO_3$ was found to shift the high-temperature cubic phase of $BaTiO_3$ to lower temperatures. At room temperature large electrostrictive coefficient up to 0.0452 $m^4\ C^{-2}$ was obtained in BT–0.10ZS ceramic, which is much larger than the traditional electrostrictive material $Pb(Mg_{1/3}Nb_{2/3})O_3$ and recently reported lead-free electrostrictive systems. The large electrostrictive response of BT–xZS ceramics makes them quite potential to be applied to new solid-state actuators.

1 Introduction

Piezoelectric actuators, having significant applications in ultra-small-scale motion, fuel injectors, micro-pumps, ink cartridges medical surgery instruments, etc., attracted continuous attentions and the overall market increased with an annual growth rate of 13% [1]. The dominant materials utilized in piezoelectric actuators are the lead-based solid solutions represented by $Pb(Zr,Ti)O_3$ (PZT) [1]. Nevertheless, the lead is toxic, and developing new lead-free alternative that can replace the PZT system has received great interest recently [2–7]. During the reported lead-free piezoelectric systems, the KNN-based solid solution suffered from the problem of strong temperature-dependent piezoelectric response while the BNT-based systems were always accompanied with large strain hysteresis [2]. An alternative way is to developing lead-free electrostrictive system, which has the distinguished advantages of good temperature stability, no poling requirement and fast response [8, 9].

Recently much progress has been made in developing lead-free electrostrictive alternatives. High-strain lead-free electrostrictors were proposed in BNT–BT–KNN, BTZ–BCT, BNT–BT–BFO and $NaNbO_3$–$BaTiO_3$ solid solutions, which can provide high strain and minimal losses at room temperature combined with minimal temperature dependence [8, 10–12]. The electrostrictive coefficient was improved from 0.022 to 0.046 $m^4\ C^{-2}$, exhibiting quite potential in high-precision ceramic actuators. It is, therefore, quite interesting and necessary to search for more high-performance lead-free electrostrictors for solid-state actuator applications.

In recent study, a novel solid solution $ZnSnO_3$ was theoretically proposed and experimentally synthesized [13, 14]. The calculated polarization P was up to 59 $\mu C\ cm^{-2}$, which is a promising lead-free candidate. Nevertheless, the pure $ZnSnO_3$ could only be synthesized under high-pressure conditions (the mixture of stoichiometric amounts of ZnO and SnO_2 could react in a high-pressure apparatus at 7 GPa and 1000 °C for 30 min and then the apparatus was quenched to room temperature) which caused great inconvenience for practical applications. An alternative routine was to design and form new solid solution. Under these considerations, a binary solid solution $(1-x)BaTiO_3$–$xZnSnO_3$ (BT–xZS), exhibiting excellent electrostrictive response, was designed and fabricated through the introduction of $ZnSnO_3$ into a typical lead-free system of $BaTiO_3$. The influences of $ZnSnO_3$ substitution on the structure, dielectric, piezoelectric, ferroelectric, electrostrictive properties, and the phase transition characteristics were investigated. It's worth noting that at a critical composition x of 0.10, large electrostrictive coefficient as high as 0.0452 $m^4\ C^{-2}$ was obtained under a moderate field of 4 kV mm^{-1} around room temperature. The excellent electrostrictive performance makes the BT–xZS system great potential in environmental-friendly solid-state actuator.

✉ Yinyin Zhu
408125415@qq.com

[1] Shanghai Normal University, Shanghai 200234, China

2 Experimental

The BT–xZS (x = 0, 0.02, 0.05, 0.07, 0.10, 0.12, 0.15) solid solution was fabricated via conventional solid-state reaction method. The starting raw materials were weighed and milled for 6 h followed by calcination at 1100 °C for 2 h. Then the powder was ball milled again for 6 h. The obtained powders were then pressed into disks and finally sintered at 1300–1350 °C for 2 h. The specimens were covered with electrode and poled in silicone oil under 4 kV mm^{-1}.

The crystal structures were characterized by X-ray diffractometry (D8 Focus, Germany) using unpoled crushed sintered samples. The dielectric constant ($\varepsilon_{33}^T/\varepsilon_0$) and loss (tan$\delta$) were measured using an automatic acquisition system with an impedance analyzer (Agilent HP4294A, Santa Clara, CA, USA). The ferroelectric hysteresis loops and strain curves were measured in silicon oil at 10 Hz with the aid of a ferroelectric analyzer (TF2000 analyzer, Aixacct, Aachen, Germany) along with a laser interferometer. The ferroelectric domain structure was characterized by piezoresponse force microscopy (PFM, MFP-3D, Asylum Research, USA).

3 Results and discussion

The measured X-ray diffraction (XRD) patterns for the BT–xZS ceramics with x from 0 to 0.15 in the 2θ range of 20°–70° are shown in Fig. 1a. From Fig. 1a, all the compositions exhibited typical perovskite structure. Careful observation revealed that there existed a small amount of second phase in the 2θ angle of 33.6° for the compositions x of 0.12 and 0.15. For the sintering temperature range up to 1350 °C, the second phase could still be detected. Higher temperature and high pressure may be required to obtain pure phase structure for the compositions $x > 0.12$. From Fig. 1b, it can be found that the introduction of the $ZnSnO_3$ caused the crystal lattice distortion and shifted the diffraction peaks towards lower 2θ direction due to larger crystal spacing of $ZnSnO_3$. For pure $BaTiO_3$ ceramics, obvious splitting could be observed for (100) and (200) peaks, indicating the ferroelectric tetragonal phase at room temperature. The substitution of $ZnSnO_3$ weakened the tetragonal distortion and induced the formation of pseudocubic or cubic structure characterized by no peak splitting for both (111) and (200) peaks.

Figures 2 and 3 show the composition, temperature, and frequency dependence of dielectric constant ($\varepsilon_{33}^T/\varepsilon_0$) and loss (tan$\delta$) for the unpoled and poled BT–xZS ceramics. Four representative compositions x of 0.02, 0.05, 0.07, and 0.10 are shown here. Compared to the normal ferroelectric $BaTiO_3$ with sharp ferroelectric to cubic phase transition peak, diffused phase transition process characterized by the broad dielectric peaks can be well observed after the introduction of the $ZnSnO_3$. However, little frequency dispersion in the dielectric constant and loss could be detected in both unpoled and poled ceramics which is different from those of the $Bi_{0.5}Na_{0.5}TiO_3$–$BaTiO_3$ system [3–5]. A schematic phase diagram was constructed for poled BT–xZS ceramics as shown in Fig. 4. The T_m was shifted to low temperatures as the $ZnSnO_3$ concentration increased. At a critical composition of BT–0.10ZS, the T_m was located around room temperature, indicating that the cubic phase became the dominant one.

Figure 5 shows the room-temperature ferroelectric P–E loops, and electric-field-induced bipolar strain curves for the pure $BaTiO_3$ ceramic. Typical rectangular P–E loop along with butterfly-shaped strain curve could be observed, indicating the strong ferroelectric long-range-order. Figure 6 shows four representative room-temperature

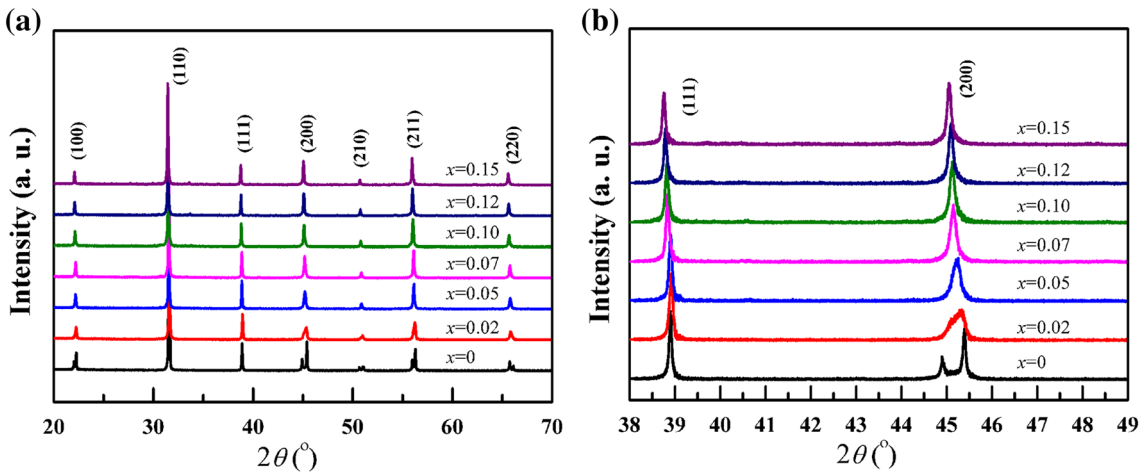

Fig. 1 XRD patterns of the BT–xZS ceramics with x from 0 to 0.15 in the 2θ range of **a** 20°–70° and **b** 38°–49°

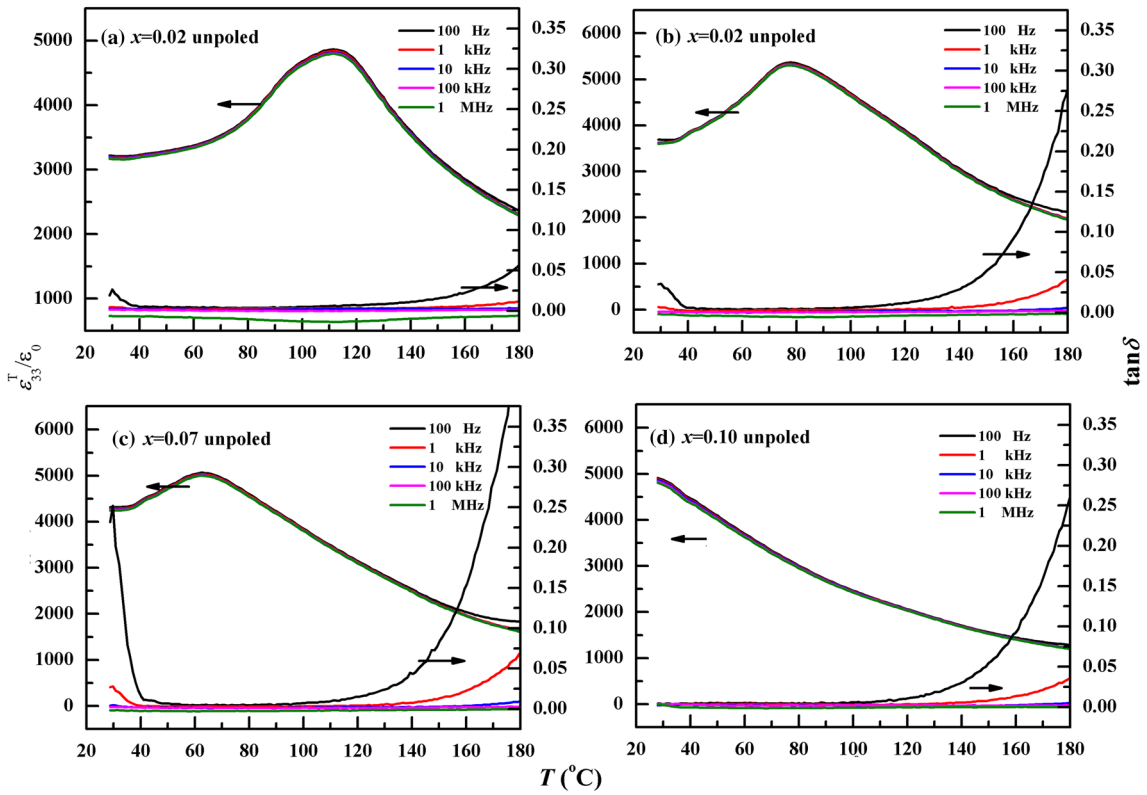

Fig. 2 The composition, temperature, and frequency dependence of dielectric constant ($\varepsilon_{33}^T/\varepsilon_0$) and loss (tan$\delta$) for the unpoled BT–$x$ZS ceramics

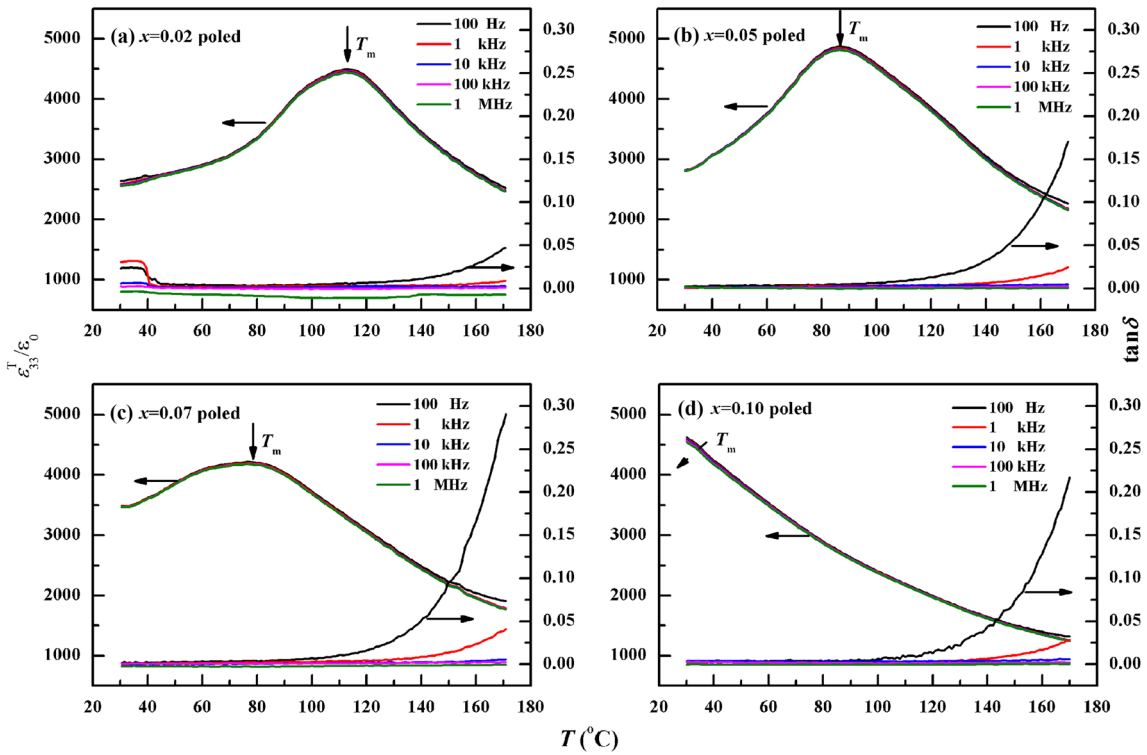

Fig. 3 The composition, temperature, and frequency dependence of dielectric constant ($\varepsilon_{33}^T/\varepsilon_0$) and loss (tan$\delta$) for the poled BT–$x$ZS ceramics

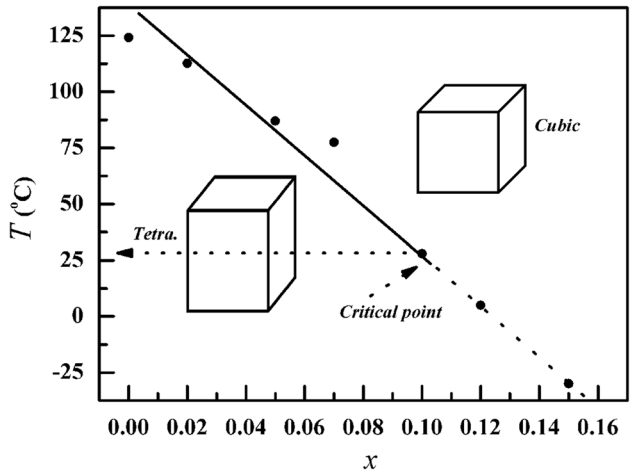

Fig. 4 A schematic phase diagram for the poled BT–*x*ZS ceramics

ferroelectric *P*–*E* loops, and electric-field-induced bipolar strain curves for BT–*x*ZS with *x* of 0.02, 0.05, 0.07, and 0.10 at 10 Hz. From Fig. 6a, after the introduction of the $ZnSnO_3$, the ferroelectric long-range-order was disrupted characterized by the sharply decreased remnant polarization and coercive field. All the compositions of the BT–*x*ZS ceramics exhibited weak ferroelectric polarization and the *P*–*E* loops became slimmer slightly with the compositions increasing. The slightly nonlinear *P*–*E* loops under the fields of 4 kV mm^{-1} were slimmer than that of other lead-free or lead-containing electrostrictors [9, 10]. On the other hand, the *S*–*E* curves show very little hysteresis with strain value in the range of 0.022–0.033% as shown in Fig. 6b and the strain value decreased gradually with the compositions increasing. To give an insight into the intrinsic mechanism for the ferroelectric and strain properties evolution, PFM was further utilized to measure the domain structure in nanoscale. Figure 7 shows the domain structures for the BT–*x*ZS system with *x* of 0 and 0.10. Clear contrast and apparent fingerprint pattern ferroelectric domains with the domain length up to ~ 2 μm could be observed for pure $BaTiO_3$, consistent with strong ferroelectric long-range-order from the *P*–*E* loop in Fig. 5a. In comparison, the BT–0.10ZS exhibited quite weak contrast from the PFM phase image. Only a small fraction of dark contrast could be detected. The results indicated that after the $ZnSnO_3$ substitution, the ferroelectric domain structure with the size of micrometer was destroyed. A phase transformation from ferroelectric tetragonal phase with typical ferroelectric domain structure to near "non-ferroelectric" state was induced. Combined with the dielectric spectrum shown in Figs. 2 and 3, it can be concluded that the high-temperature cubic phase was shifted downwards. Therefore, the remnant polarization and strain value decreased substantially. In addition, from Fig. 6a, the energy content in the ferroelectric hysteresis loop decreased with the composition *x* increasing and a purely electrostrictive response was induced in the critical composition BT–0.10ZS.

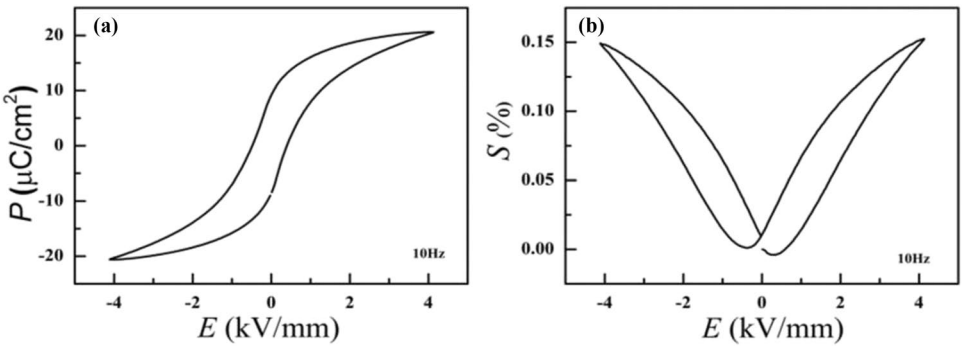

Fig. 5 Room-temperature ferroelectric *P*–*E* loops, and electric-field-induced bipolar strain curve for pure $BaTiO_3$ ceramic

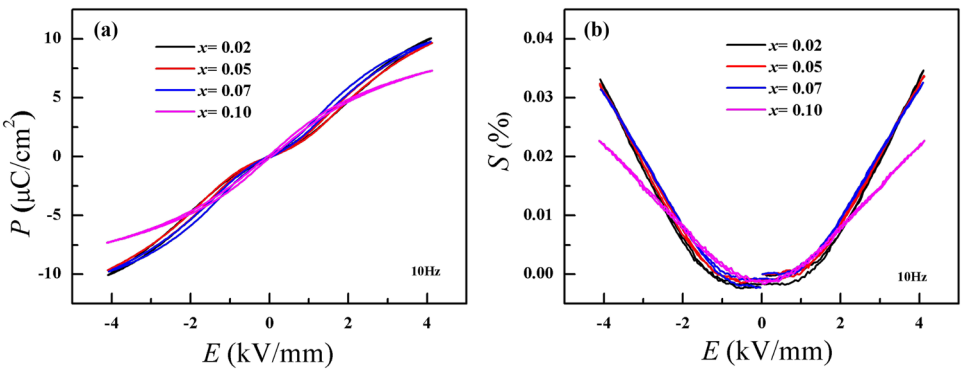

Fig. 6 Four representative room-temperature ferroelectric *P*–*E* loops, and electric-field-induced bipolar strain curve for BT–*x*ZS with *x* of 0.02, 0.05, 0.07, and 0.10 at 10 Hz

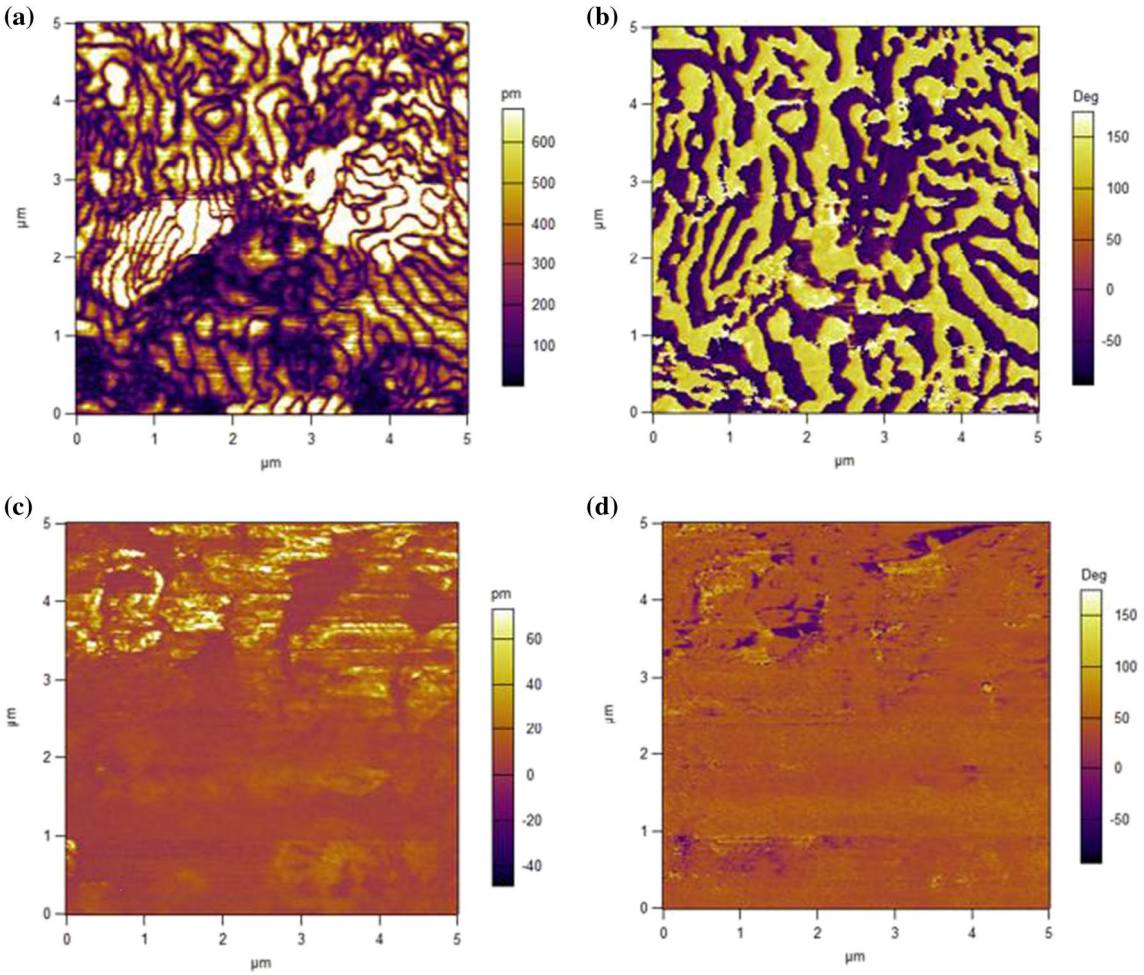

Fig. 7 The room-temperature domain patterns for the BT–*x*ZS system with **a**, **b** for $x = 0$ and **c**, **d** for $x = 0.10$

Figure 8 shows the relations of the strain responses vs. the square of the ferroelectric polarization. A linear relation could be found, indicating an electrostrictive behavior and the electrostrictive coefficient Q could be obtained from the following formula,

$$S = QP^2, \quad (1)$$

where the S and P were the electric-field-induced strain and ferroelectric polarization, respectively. Obviously, the S–P^2 curves for all the compositions were linear, which meant all the compositions were pure electrostrictors. The electrostrictive coefficient Q was calculated to be 0.0328 m^4 C^{-2}, 0.0339 m^4 C^{-2}, and 0.0342 m^4 C^{-2} for the compositions x of 0.02, 0.05, 0.07, respectively. It is worth noting that the largest electrostrictive coefficient Q was obtained for BT–0.10ZS with the value up to 0.0452 m^4 C^{-2}. This value is superior to the well-known electrostrictive material $Pb(Mg_{1/3}Nb_{2/3})O_3$ (PMN) of 0.017 m^4 C^{-2} and notably larger than that of the recently reported BNT–BT–KNN, BNT–BT–KN, BTZ–BCT, etc. [8, 11, 12, 15, 16]. The

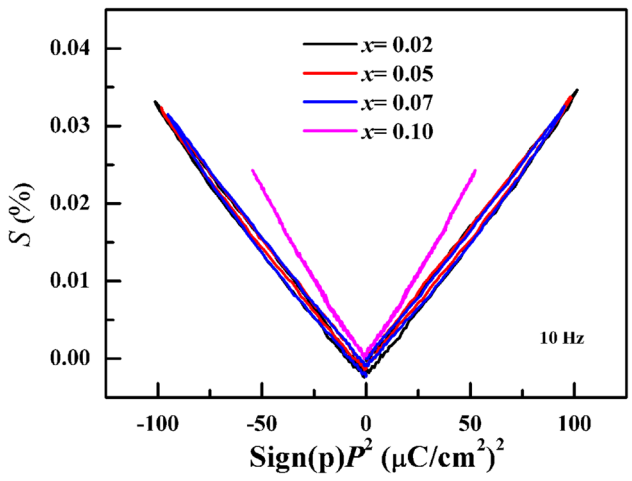

Fig. 8 The strain curve vs. the square of the polarization for the BT–*x*ZS ceramics under the electric field of 4 kV mm^{-1} at 10 Hz

excellent electrostrictive response makes BT–xZS quite potential in solid-state actuators applications.

4 Conclusions

In this paper, a new lead-free electrostrictive solid solution BT–xZS was proposed. The introduction of $ZnSnO_3$ was found to shift the high-temperature cubic phase to low temperature, accompanying by the weakened ferroelectric polarization and domain pattern. At a critical composition x of 0.10, high electrostrictive coefficient Q as high as 0.0452 m^4 C^{-2} can be obtained at room temperature, much larger than that of the well-known PMN and other lead-free electrictrictors. This makes BT–xZS quite potential in lead-free high-precision solid-state actuators.

Acknowledgements Thanks very much for the continuous support from Prof. Dazhi Sun in the Department of Chemistry, Shanghai Normal University.

References

1. W. Jo, R. Dittmer, M. Acosta, J.D. Zang, C. Groh, E. Sapper, K. Wang, J. Rödel, J. Electroceram. **29**, 71 (2012)
2. J. Rödel, W. Jo, K.T.P. Seifert, E.M. Anton, T. Granzow, D. Damjanovic, J. Am. Ceram. Soc. **92**, 1153 (2009)
3. F.F. Wang, M. Xu, Y.X. Tang, T. Wang, W.Z. Shi, C.M. Leung, J. Am. Ceram. Soc. **95**, 1955 (2012)
4. F.F. Wang, C.M. Leung, Y.X. Tang, T. Wang, W.Z. Shi, J. Appl. Phys. **114**, 164105 (2013)
5. Q.R. Yao, F.F. Wang, F. Xu, C.M. Leung, T. Wang, Y.X. Tang, X. Ye, Y.Q. Xie, D.Z. Sun, W.Z. Shi, A.C.S. Appl, Mater. Interfaces **7**, 5066 (2015)
6. X.M. Liu, X.L. Tan, Adv. Mater. **28**, 574 (2016)
7. C. Groh, D.J. Franzbach, W. Jo, K.G. Webber, J. Kling, L.A. Schmitt, H.J. Kleebe, S.J. Jeong, J.S. Lee, J. Rödel, Adv. Funct. Mater. **24**, 356 (2014)
8. R.Z. Zuo, H. Qi, J. Fu, J.F. Li, M. Shi, Y.D. Xu, Appl. Phys. Lett. **108**, 232904 (2016)
9. C. Ang, Z. Yu, Adv. Mater. **18**, 103 (2006)
10. S.T. Zhang, A.B. Kounga, W. Jo, C. Jamin, K. Seifert, T. Granzow, J. Rödel, D. Damjanovic, Adv. Mater. **21**, 4716 (2009)
11. D. Duraisamy, G.N. Venkatesan, Appl. Phys. Lett. **112**, 052903 (2018)
12. F. Li, L. Jin, R.P. Guo, Appl. Phys. Lett. **105**, 232903 (2014)
13. M. Nakayama, M. Nogami, M. Yoshida, T. Katsumata, Y. Inaguma, Adv. Mater. **22**, 2579 (2010)
14. Y. Inaguma, M. Yoshida, T. Katsumata, J. Am. Chem. Soc. **130**, 6704 (2008)
15. J.M. Li, F.F. Wang, X.M. Qin, M. Xu, W.Z. Shi, Appl. Phys. A **104**, 117 (2011)
16. A. Furuta, K. Uchino, J. Am. Ceram. Soc. **76**, 1615 (1993)